IEEE Access
Multidisciplinary ⋮ Rapid Review ⋮ Open Access Journal

Received 9 December 2022, accepted 19 December 2022, date of publication 22 December 2022, date of current version 5 January 2023.

Digital Object Identifier 10.1109/ACCESS.2022.3231688

RESEARCH ARTICLE

Self-Adaptive Overtemperature Protection Materials for Safety-Centric Domestic Induction Heating Applications

A. PASCUAL[1], (Graduate Student Member, IEEE), J. ACERO[1], (Senior Member, IEEE), S. LLORENTE[2], C. CARRETERO[3], (Senior Member, IEEE), AND J. M. BURDIO[1], (Senior Member, IEEE)

[1]Department of Electronic Engineering and Communications, University of Zaragoza, 50018 Zaragoza, Spain
[2]Bosch-Siemens Home Appliances Group, Department of Research and Development, 50016 Zaragoza, Spain
[3]Department of Applied Physics, University of Zaragoza, 50009 Zaragoza, Spain

Corresponding author: A. Pascual (a.pascual@unizar.es)

This work was supported in part by the Spanish MICINN under Projects AEI under Grant PID2019-103939RB-I00, Grant PDC2021-120898-I00, Grant TED2021-129274B-I00, Grant CPP2021-008938, and Grant ISCIII PI21/00440; and in part by EU through FEDER and NextGenerationEU/PRTR Programs, by the DGA-FSE, and by the BSH Home Appliances Group.

ABSTRACT Security aspects in the household sphere have become a major concern in modern societies. In particular, regardless of the technology used, users increasingly appreciate a protection system to prevent material damage in the case of human errors or distractions during the cooking process. This paper presents a sensorless method for detecting and limiting overtemperature, unique to induction cooktops, based on their specific features, such as automatic pot detection and load power factor estimation. The protection system exploits the change in the load material properties at certain temperatures, the effect of which may be enhanced by arranging a multilayer structure comprising a low Curie temperature alloy and an aluminum layer. The proposed multilayer load exhibits two differentiated states: a normal state, where the cookware is efficiently heated, and a protection state, above the safety temperature, where the power factor abruptly decreases, limiting the overheating and making the state easily detectable by the cooktop. This method of overtemperature self-protection uses the electronics of conventional induction cooktops; therefore, no other sensors or systems are required, reducing its complexity and costs. Simulation and experimental results are provided for several cookware designs, thereby proving the feasibility of this proposal.

INDEX TERMS Home appliances, induction heating, domestic safety, electromagnetic properties.

I. INTRODUCTION

In the last decade, induction has become the preferred heating technology for domestic use in many countries [1]. Compared to traditional cooking systems, such as gas or radiant cooktops, it has significant advantages [2], which include higher efficiency [3], [4] and safety [5], increased flexibility [6], faster heating, and, in addition, it is free of combustion and emissions. The domestic induction heating (DIH) systems, illustrated in Fig. 1, are composed of the power electronics converter and the inductor-load system, which is usually modeled as an equivalent resistance R_{eq}, connected in series with an equivalent inductance, L_{eq} [7], [8]. These parameters determine the power factor of the load and, consequently, the delay between current and voltage in the load.

In cooking processes it is important to keep cooktop temperature in a safe range, as distractions or inexperience can lead to property damage and fires in the kitchen. According to [9], in the US from 2014 to 2018 there has been an average of 4820 injuries and more than 1 billion dollars in losses due to fires in the kitchen. For this reason, DIH incorporate an overtemperature protection system that cuts off the power supply when the temperature exceeds a threshold.

The associate editor coordinating the review of this manuscript and approving it for publication was Sze Sing Lee.

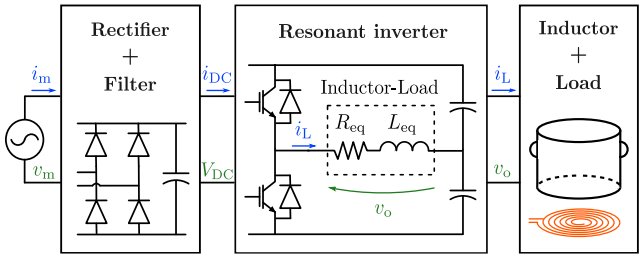

FIGURE 1. Typical scheme of the power electronics of an induction cooktop.

The most challenging task in developing safety systems for induction cooktops is to obtain an accurate value of the cookware temperature. Typically, this temperature is estimated from the measurements of an NTC thermistor located in the center of each inductor, which measures the temperature of the lower part of the ceramic glass [10], [11]. However, the ceramic glass filters the cookware temperature, so the estimation of the cookware temperature differs (with different time constants and gains) depending on the location of the measurement point, the position and shape of the cookware base, and the heat transferred between the cookware and the ceramic glass. Consequently, the behavior of the sensor is variable and uncertain, requiring the introduction of complex mathematical models and estimation algorithms to obtain an approximation of the pot temperature. In addition, if the thermal contact between the cookware and the ceramic glass is poor the heat transfer is reduced, so the algorithm may not detect the overtemperature in time [12]. Finally for solutions such as the flexible cooking surface [5] a thermistor is used in each inductor complicating the cooktop design, and in the proposals for cooking underworktop, where the ceramic glass is removed [13], this method does not work.

Therefore, in recent years, temperature measurement in cookwares has been the subject of several studies. For instance, the use of inductive temperature sensors provides the temperature of the vessel by measuring changes in the impedance of a sensing coil [14]. Nevertheless, it requires an additional circuitry and does not have enough accuracy. There are also infrared sensors, which provide non-contact and instantaneous temperature measurements [15]. However, they are usually also placed under the ceramic glass and the measurements depend on many parameters, that may vary with use. Consequently, current protection solutions based on the aforementioned systems are not optimal and still have several areas for improvement.

This paper presents a solution for overtemperature detection in DIH based on the power factor variations with temperature of a especial load arranged by means of a multilayer structure made of aluminum and ferromagnetic materials, whose Curie temperature (T_{Curie}) coincides with the safety temperature threshold. Above this temperature, the ferromagnetic layer loses its magnetic properties and this fact combined with the presence of the aluminum results in a considerable change of the power factor. The cooktop's power electronics can easily detect the variations in the PF [16], which together with the multilayer load would allow detection of overtemperature. This method shares the same principle as the automatic pot detection system [17], [18], integrated into the induction cooktops since its first commercial versions. Thus, this method adds self-protection functionality against overtemperature to the cooktop power electronics and can be integrated directly into any induction cooktop without modifying its hardware, reducing its complexity and costs.

Concerning our preliminary work [19], this paper contributes an advanced study of the multilayer load arrangements for induction heating, a theoretical analysis of the magnetic model, facilitating the design and choice of materials, and extends the preliminary experimental results.

The paper is organized as follows: Section II shows an analytical magnetic model for multilayer loads and analyzes the influence of this arrangement on the inductor-load equivalent circuit. Section III presents the material selection and the design of the load for the overtemperature protection system. Section IV present the experimental setup and the results. Finally, some conclusions are drawn in Section V.

II. EQUIVALENT CIRCUIT OF A MULTILAYER INDUCTOR-LOAD SYSTEM

The inductor-load system, illustrated in Fig. 1, is usually electrically modeled as an equivalent circuit with a resistance R_{eq} and an inductance L_{eq} in series, establishing an analogy with a transformer, in which the inductor coil represents the primary winding and the cooking vessel acts as the core and secondary winding of the transformer. In this circuit the resistance R_{eq} represents the power dissipated in the system and L_{eq} represents the magnetic field of the system. The equivalent circuit depends on many parameters as the number of turns of the coil, the coil geometry and diameter, the arrangement and size of the ferrites, the operating frequency, the load geometry, the relative magnetic permeability (μ_r) and the electrical conductivity (σ) of the load, among others [20]. In addition, the use of loads with multiple layers is becoming more and more common, which also has an impact on the inductor-load equivalent circuit.

A. ANALYTICAL MODEL FOR MULTILAYER STRUCTURES

The multilayer loads can be modeled in terms of R_{eq} and L_{eq}. The model used in this work is based on the solution of Maxwell's equations for a set of n concentric filamentary currents placed between two multilayer media. In this work, in addition to the finite element tools normally used in induction heating [21], [22], [23], [24], it has been used analytical models because multilayer arrangements can include very thin layers (about tens of microns) which require appropriate meshing, increasing the computational cost. Moreover, studying the influence of layer thickness using FEM requires re-meshing each simulation, which also increases the processing time.

The system under study is shown in Fig. 2. Considering axial symmetry, the coil is placed at $z = 0$ and each filamentary turn carries a current $\hat{I}e^{j\omega t}$, where $\hat{I}$ is the amplitude and ω

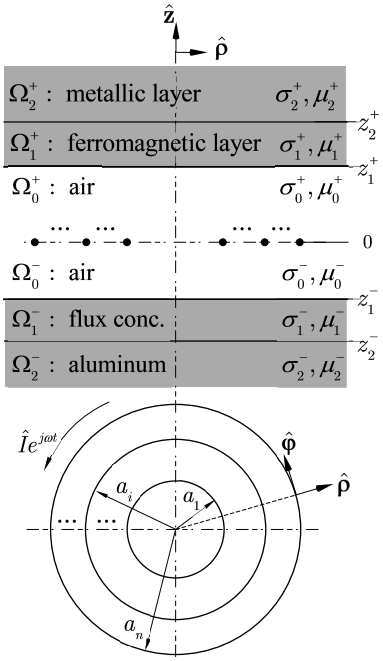

FIGURE 2. Model of the considered induction heating system.

is the angular frequency. The multilayer media comprises the induction load, the ferrite bars and the aluminum shielding. The induction load consists of two stacked layers, the lowest layer corresponds to a ferromagnetic material and the other layer is a good conductive material, for instance, aluminum. The equivalent impedance of this system can be obtained by assuming the following simplifications [25], [26]:

- The system presents axial symmetry.
- Layers are semi-infinite in the horizontal dimension.
- Materials are linear, homogeneous and isotropic and are characterized by means of the electrical conductivity, σ, and the magnetic permeability, μ_r.
- At the interest frequency range, from 20 kHz to 75 kHz, capacitive or radiative effects are negligible.
- The flux concentrator has been modeled as a disk whose μ_r is equivalent to that of ferrite bar arrangements.

The equivalent impedance of the induction systems is the sum of two parts: first, the impedance of the coil in the air Z_{air}, and second the contribution of the multilayer, Z_{media}. Consequently:

$$Z_{\text{eq}} = Z_{\text{air}} + Z_{\text{media}} \tag{1}$$

The first term is purely inductive due to the adopted ideal filamentary model and, consequently, it doesn't capture the resistance of windings. Therefore, Z_{air} represents the self-inductance of the coil which can be obtained as follows [27]:

$$Z_{\text{air}} = j\omega\pi\mu_0 \int_0^\infty G(\beta a)\, d\beta \tag{2}$$

where β is an integration variable and $G(\beta a)$ is a geometrical function which accounts for the geometry of the coil, and it is defined as follows:

$$G(\beta a) = \sum_{i=1}^{n}\sum_{j=1}^{n} a_i a_j J_1(\beta a_i) J_1(\beta a_j) \tag{3}$$

where a_i, a_j are the radii of the i^{th} and j^{th} turns, respectively, J_1 is the Bessel function of the first kind and order one.

The contribution of the media can be obtained by particularizing the general case of a planar coil between two multilayer media [25] to the system under study. This contribution is:

$$Z_{\text{media}} = j\omega\pi\mu_0 \int_0^\infty \left[\frac{\phi_t e^{-\beta d_t}}{1-\phi_t\phi_b e^{-2\beta(d_t+d_b)}} + \frac{\phi_b e^{-\beta d_b} + 2\phi_t\phi_b e^{-2\beta(d_t+d_b)}}{1-\phi_t\phi_b e^{-2\beta(d_t+d_b)}} \right] G(\beta a)\, d\beta \tag{4}$$

where d_t and d_b are the distances from the coil to the top and bottom multilayers, respectively. According to Fig. 2 these distances are:

$$\begin{aligned} d_t &= z_1^+ \\ d_b &= -z_1^- \end{aligned} \tag{5}$$

Moreover, ϕ_t and ϕ_b are two characteristic magnitudes of the top and bottom multilayer media. These magnitudes depend on the properties of each layer through the following parameter:

$$\eta_k^{\pm} = \left(\beta^2 + j\omega\sigma_k^{\pm}\mu_k^{\pm}\right)^{\frac{1}{2}} \tag{6}$$

where $\sigma_k^{\pm}$, $\mu_k^{\pm}$ are the electrical conductivity and magnetic permeability of the $k^{\text{th}}-$layer. According to these definitions and the results of [25], for this particular case ϕ_t and ϕ_b are defined as follows:

$$\begin{aligned} \phi_t = &\left[\left(\beta\mu_{r1}^+ + \eta_1^+\right)\left(\mu_{r2}^+\eta_1^+ - \mu_{r1}^+\eta_2^+\right) e^{-\eta_1^+ t_l} \right. \\ &\left. + \left(\beta\mu_{r1}^+ - \eta_1^+\right)\left(\mu_{r2}^+\eta_1^+ + \mu_{r1}^+\eta_2^+\right) e^{\eta_2^+ t_l} \right] \\ &\times \left[\left(\beta\mu_{r1}^+ - \eta_1^+\right)\left(\mu_{r2}^+\eta_1^+ - \mu_{r1}^+\eta_2^+\right) e^{-\eta_1^+ t_l} \right. \\ &\left. + \left(\beta\mu_{r1}^+ + \eta_1^+\right)\left(\mu_{r2}^+\eta_1^+ + \mu_{r1}^+\eta_2^+\right) e^{\eta_2^+ t_l} \right]^{-1} \end{aligned} \tag{7}$$

and

$$\begin{aligned} \phi_b = &\left[\left(\mu_{r1}^- - 1\right)\left(\beta + \mu_{r1}^-\eta_2^-\right) e^{-\beta t_f} \right. \\ &\left. + \left(\mu_{r1}^- + 1\right)\left(\beta - \mu_{r1}^-\eta_2^-\right) e^{\beta t_f} \right] \\ &\times \left[\left(\mu_{r1}^- + 1\right)\left(\beta + \mu_{r1}^-\eta_2^-\right) e^{-\beta t_f} \right. \\ &\left. + \left(\mu_{r1}^- - 1\right)\left(\beta - \mu_{r1}^-\eta_2^-\right) e^{\beta t_f} \right]^{-1} \end{aligned} \tag{8}$$

where t_l and t_f are the thickness of the ferromagnetic layer and the ferrite, respectively, and according to Fig. 2 they are defined as follows:

$$\begin{aligned} t_l &= z_2^+ - z_1^+ \\ t_f &= z_1^- - z_2^- \end{aligned} \tag{9}$$

Moreover, it should be taken into account that the magnetic permeability has nonlinear dependencies with the magnetic

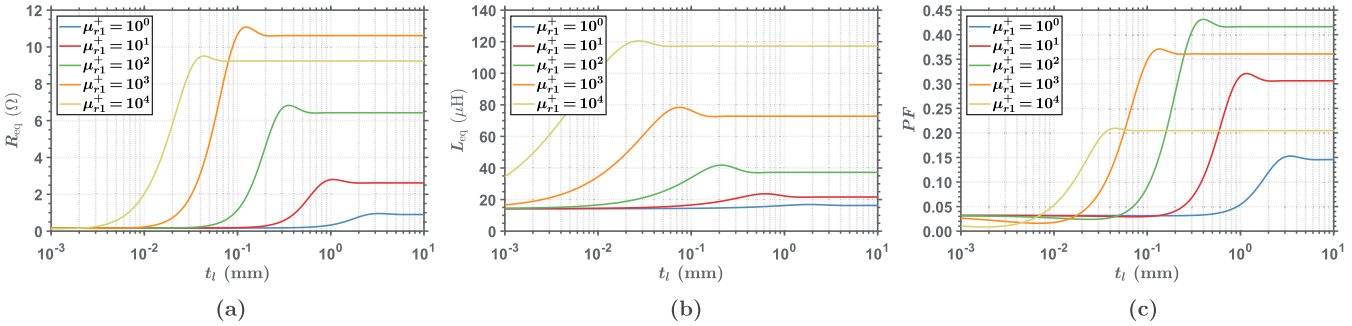

FIGURE 3. Effect of the thickness and the properties of the ferromagnetic layer material on the equivalent impedance ((a) equivalent resistance, (b) equivalent inductance and (c) power factor) of a typical inductor-load system.

field strength (H) and temperature, so the Z_{eq} varies as the load heats up. Therefore, to simulate the behavior of the equivalent impedance in the case of cookware overheating, it has been considered that the variation of the electrical conductivity with temperature in the range of interest of the application of induction heating is negligible, and the power distribution and temperature increment is uniform at all points of the load. Thus, the only parameter that varies in the case under study is the μ_{r1}^+ with respect the temperature and the magnetic field. So, the analytical model can simulate the cookware overheating by performing a sweep for different values of μ_{r1}^+(T, H) within the temperature range of interest and in which each value of μ_{r1}^+ corresponds to a specific value of H and Temperature. Finally, the magnetic field strength can be obtained from the current circulating through the inductor. Which, by knowing the switching frequency and the equivalent impedance, can be obtained from the analysis of the half-bridge resonant inverter shown in Fig. 1.

B. ANALYSIS OF THE MULTILAYER ARRANGEMENT

Based on the analytical model, it has been analyzed the dependence of the bottom layer parameters on the Z_{eq} of a typical inductor-load system. The analysis was performed at an operating frequency of 60 kHz and using a 24-turn planar coil with the same diameter as the load ($\phi_{coil} = \phi_{load} = 150$ mm). The multilayer load comprises two layers: The bottom layer is a material with $\sigma_1^+ = 10^6$ S/m and different values of relative magnetic permeability, while the metallic layer corresponds to aluminum ($\sigma_2^+ = 3 \cdot 10^7$ S/m, $\mu_{r2}^+ = 1$).

Fig. 3 (a) shows that R_{eq} strongly depends on the permeability and thickness of the bottom layer. When the μ_{r1}^+ is low, the power dissipation achieved by the Joule effect, and hence the R_{eq} is also low. Furthermore, for low magnetic permeabilities and thicknesses less than 1 mm the R_{eq} is close to zero, which means that the load barely heats up. Fig. 3 (b) shows that the higher relative magnetic permeability the more inductive the system is, increasing the L_{eq}. Finally, Fig. 3 (c) shows the dependence of the power factor ($PF = R_{eq}/|Z_{eq}|$) on the bottom layer characteristics. This power factor is associated with the phase difference between the voltage and the current in the inverter and is

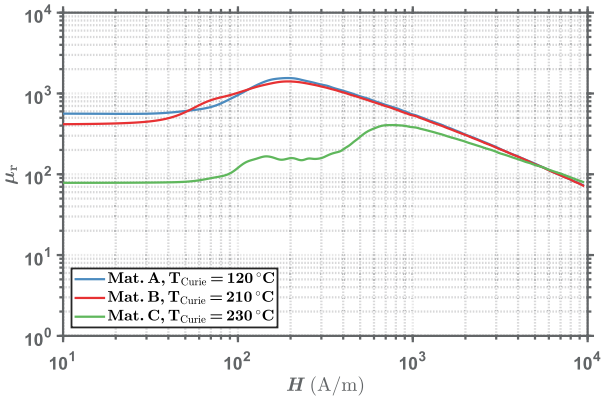

FIGURE 4. μ_r versus H in the low curie temperature alloys.

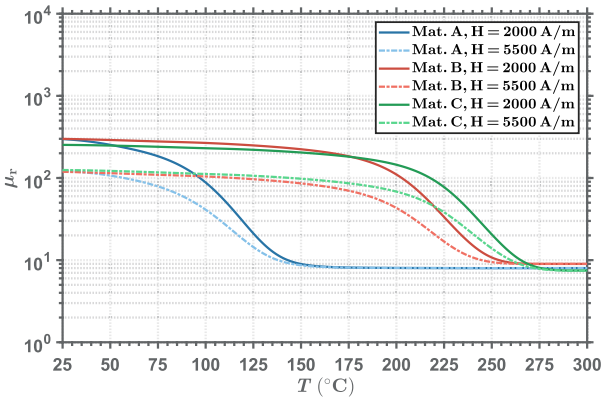

FIGURE 5. μ_r versus temperature in the low curie temperature alloys.

the parameter currently used in the automatic pot detection system. It can be observed that with a bottom layer thickness greater than 0.1 mm and composed of a ferromagnetic material with a μ_{r1}^+ between 100 and 1000 the load could be heated with a high PF. Similarly, for μ_{r1}^+ lower than 10 and t_l smaller than 1 mm, the R_{eq} is almost zero and the PF drops considerably.

Thus, by using a material that can switch between these two μ_{r1}^+ states and with a t_l between 0.1 mm and 1 mm, it would allow the load to have 2 states: one state in which it

can be heated efficiently and a second state, at low μ_{r1}^{+}, where the low R_{eq} limits its overheating and the decrease in the PF allows the power electronics to detect the overtemperature.

III. MATERIAL SELECTION AND LOAD STRUCTURE

The load materials should provide a balanced R_{eq} to heat it with high efficiency [28] and must also meet the requirements of high melting point and high corrosion resistance demanded by commercial cookware. In addition, to self-protect the load against high temperatures, their electromagnetic properties have to cause significant changes in the PF of the equivalent circuit at a temperature within the overtemperature detection range of interest, between 100 °C (boiling water) and 250 °C (frying). These requirements make the low temperature Curie alloys an excellent choice for this proposal.

A. LOW CURIE TEMPERATURE ALLOYS CHARACTERIZATION

The Curie temperature, present in all ferromagnetic materials, is the temperature above which a material loses its magnetization and behaves as a purely paramagnetic material. In most metals, this temperature is usually very high, i.e. in iron T_{Curie} = 768 °C, outside the range of interest of the application. Nevertheless, certain metallic alloys that, by slightly modifying their composition [29], allow to preset its Curie temperature between 100 °C and 300 °C. The information available from these alloys is limited and it is not usually known how their properties behave with respect to temperature except its Curie temperature. So, it is necessary to perform a previous characterization of the material. To obtain the dependence on temperature of the μ_r in these materials it has been followed the method proposed in [30] and [31].

The magnetic characterization at different temperatures has been carried out on three alloys that fulfill all the points mentioned above. As a result, it has been obtained the value of their relative magnetic permeability with respect to the temperature at different values of magnetic field strength; from which it is possible to simulate their nonlinear magnetic behavior with the analytical model. Fig. 4 shows the dependence of the μ_r on the magnetic field strength (H) and Fig. 5 illustrates the dependence of the μ_r with the temperature. The alloys composition and electrical conductivity at room temperature are shown in Table 1. It can be observed how the relative magnetic permeability remains constant, or slightly decreases with the temperature, until the material approaches its Curie temperature where there is a drastic drop in the μ_r. So, regarding the suitability of these materials for DIH, its μ_r allow to heat the cookware efficiently until they reaches their Curie temperature. Above this temperature the alloys have a permeability below 10, reducing their heating capabilities. However, as exposed in the next subsection by using this material alone, without the metallic layer, the changes in the PF are not significant enough to easily detect overtemperature and its R_{eq}, although low, would still allow the vessel to be heated. Therefore, the use of these materials alone is not sufficient for self-protection against high temperatures.

TABLE 1. Composition of the low curie temperature alloys.

Alloy Name	T. Curie (°C)	σ (S/m)	Composition			
			% Fe	% Ni	% Cr	% Mn
Mat. A	120	$1.12{\cdot}10^6$	66,92	30,49	2,14	0,45
Mat. B	210	$0.97{\cdot}10^6$	38,81	49,84	10,95	0,40
Mat. C	230	$0.98{\cdot}10^6$	40,24	49,03	10,29	0,44

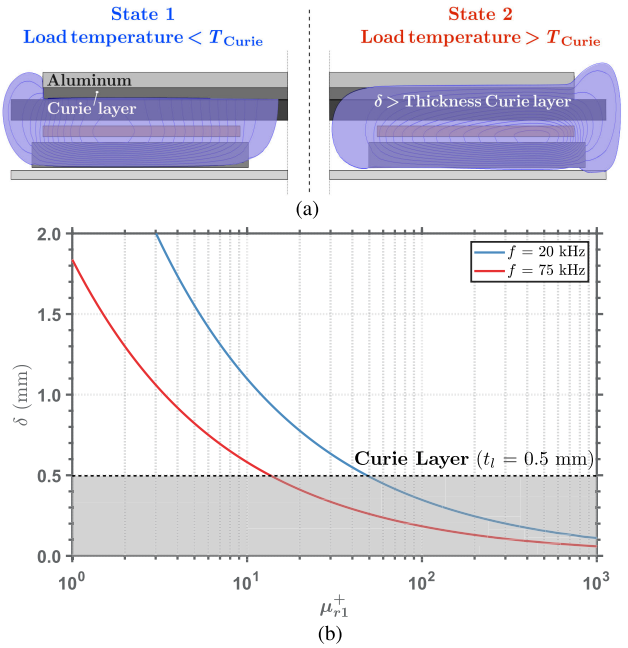

FIGURE 6. Schematic representation of the operating principle of the multilayer structure (a) and skin depth variation with μ_{r1}^{+} (b).

B. COOKWARE WITH MULTILAYER STRUCTURE

According to the results of Section II-B the variations of the equivalent resistance and power factor at the desired temperature can be enhanced by using a multilayer structure at the bottom of the cookware. This structure comprises a layer with a predefined thickness of a low Curie temperature alloy and a thicker layer of a good conductor and non-ferromagnetic material, such as aluminum, placed on top. The operating principle of the multilayer structure, illustrated in Fig. 6, and can be explained by means of the skin depth (δ), which is the distance at which a sinusoidal electromagnetic field decays the 63 % and, thus, determines the current conduction section. This distance depends on the frequency (f) and the electromagnetic properties of the material (μ_r and σ) as follows:

$$\delta = \sqrt{\frac{1}{\pi f \sigma \mu_r \mu_0}} \tag{10}$$

where μ_0 is the vacuum permeability. As depicted in Fig. 6, with proper design of the layer thickness, it can be achieved that below the Curie temperature ($\mu_{r1}^{+} > 100$) the δ does not exceed the thickness of the first layer. Thus, R_{eq} and PF are only influenced by the material of this layer. When this temperature is exceeded ($\mu_{r1}^{+} < 10$) the magnetic field

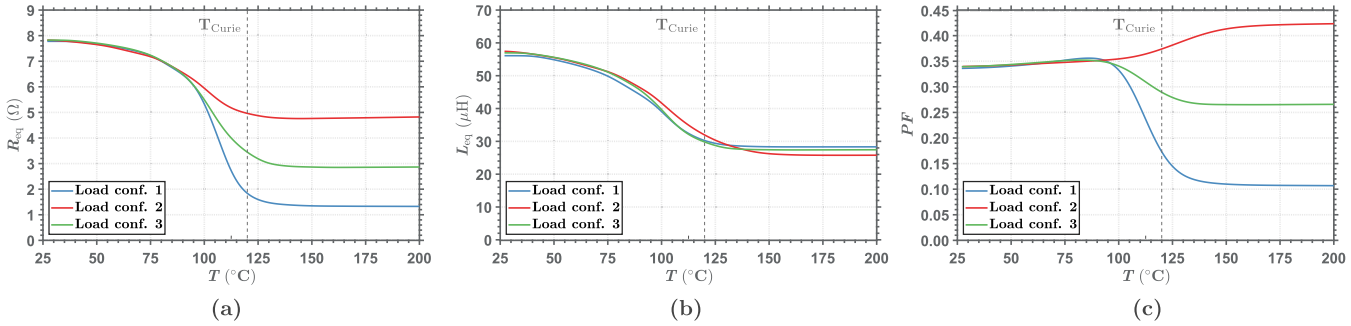

FIGURE 7. Dependence of the equivalent circuit parameters ((a) equivalent resistance, (b) equivalent inductance and (c) Power Factor) on temperature for different curie layer thickness and structures for the bottom of the cookware, at an operating frequency of 60 kHz. Load. conf 1 (Multilayer, $t_l = 0.5$ mm), Load. conf 2 (Only Curie layer, $t_l = 0.5$ mm), Load. conf 3 (Only Curie layer, $t_l = 2.5$ mm).

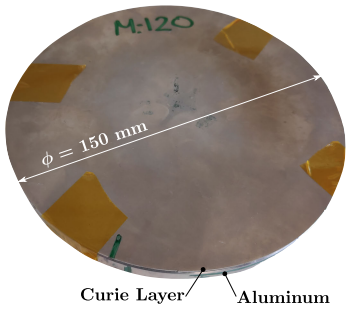

FIGURE 8. Prototype used in the experimental measurements.

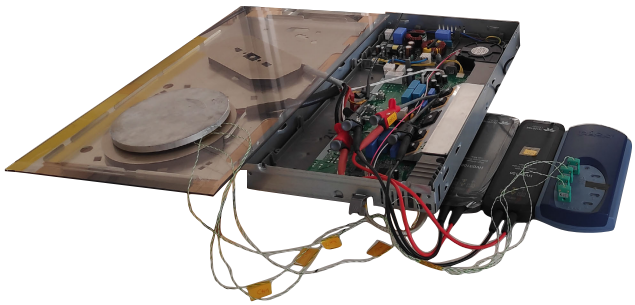

FIGURE 9. Setup used in experimental measurements.

passes through to the second layer, which is made of aluminum, causing considerable changes in the equivalent circuit. In Fig. 6(b) is shown that, with a thickness of 0.5 mm for the low Curie temperature material layer, the skin depth when the T_{Curie} is exceeded, and the μ_{r1}^{+} drops bellow 10, is higher than the t_l and allows the magnetic field to penetrate the aluminum layer in the whole range of working frequencies in DIH (20 - 75 kHz).

The variation of the circuit parameters with temperature for three different load structures is shown in Fig. 7. It has been analyzed one multilayer structure (load conf. 1), with an aluminum layer on top and a Curie layer of thickness, t_l, of 0.5 mm (less than δ when exceeding T_{Curie}) and two structures with a single curie layer of different thicknesses ranging from 0.5 mm (load conf. 2) to 2.5 mm (load conf. 3) and air on top. The model and the inductor-load configuration is the same as the analyzed in section II-B. For the Curie layer, it has been used the Mat. A of Table 1 whose μ_r changes with the temperature as shown in Fig. 5 with a H = 2000 A/m. Finally, it has been considered that the temperature of the material increases uniformly from 25 °C to 200 °C.

In Fig. 7 (a) is shown that the R_{eq} is similar for the different cookware bottom structures until they approach the T_{Curie} of the material. As it can be observed the multilayer structure presents the most significant drop in R_{eq}. In the case of the Curie layer with thickness higher than δ, as the magnetic field does not reach the aluminum, the R_{eq} drop is lower. Finally, in the case of the Curie layer with a thickness smaller than δ and without the metallic layer, the conductive area is geometrically fixed by the layer thickness instead of the skin depth, and thus the drop of R_{eq} is considerably reduced. The L_{eq} has lower variations when the material properties are not suitable for DIH, which occurs in the three structures when they exceed the T_{Curie}, so as can be seen in Fig. 7 (b) the temperature dependence is very similar for the three cases. Finally, taking into account that the criteria for selecting an appropriate multilayer structure is to achieve a significant variation of the PF the most suitable option for the bottom of the cookware, as can be seen in Fig. 7 (c), is the one with a 0.5 mm thickness in the curie material layer and the metallic layer above it.

IV. EXPERIMENTAL MEASURES

In order to verify the concept presented in the previous section, three prototypes have been constructed one for each of the Curie materials listed in Table 1. The prototypes correspond to the dimensions and geometry of a conventional pan. As shown in Fig. 8, they are composed of a thin layer of 150 mm diameter and 0.5 mm thickness of the low T_{Curie} alloy and on top an aluminum layer with the same diameter.

The setup used for experimental validation is shown in Fig. 9. The power electronics corresponds to a commercial induction cooktop with a circular inductor of 150 mm diameter. The temperature was measured using a set of

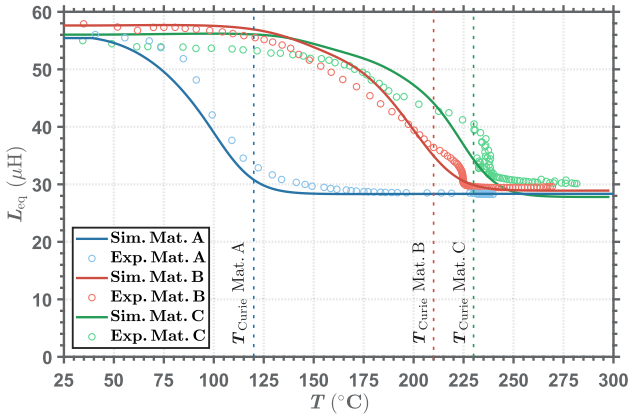

FIGURE 10. Dependence of L_{eq} on temperature at $f = 60$ kHz.

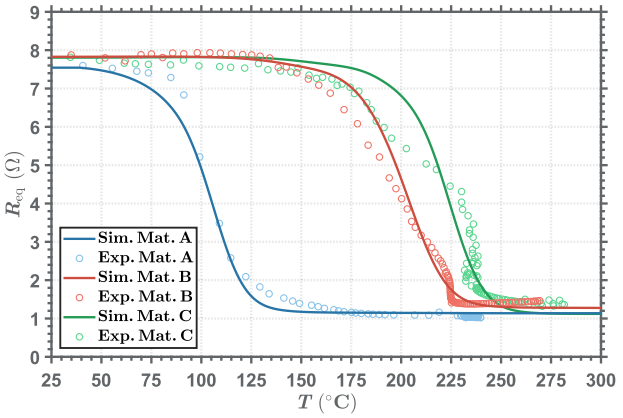

FIGURE 11. Dependence of R_{eq} on temperature at $f = 60$ kHz.

thermocouples placed along the radius of the prototype, the voltage and current of the inductor-load system was measured using a LECROY MDA805A oscilloscope and a universal diagnosis adapter (UDA) was used to control the induction cooktop and obtain certain variables calculated by the microcontroller.

A. MEASUREMENT CONDITIONS

The measurements have been carried out with the setup described above, collecting samples every second, at a working frequency of 60 kHz and applying a constant power of 350 W. The tests have been performed at low power so that the vessel heats up slowly and therefore more accurate measurements are achieved over the entire temperature range.

To obtain R_{eq} and L_{eq} it has been applied the Fourier analysis of the voltage and current in the coil and has been used first harmonic approximations, which are widely used in the study of resonant inverters [32]. The Z_{eq} can be approximated by the equivalent impedance of the first harmonic, Z_{1h}, which is calculated by obtaining the DTFS (discrete-time Fourier series) coefficients of the voltage at the coil $v_{o,1h}$ and its input current $i_{L,1h}$

$$Z_{1h} = \frac{v_{o,1h}}{i_{L,1h}} \approx Z_{eq} = R_{eq} + 2\pi f_{sw} L_{eq} \tag{11}$$

where f_{sw} is the switching frequency.

B. EXPERIMENTAL RESULTS

The comparison between calculated and measured results are shown in Fig. 10, Fig. 11, Fig. 12 and Fig. 13. From Fig. 10 it can be noted that the equivalent inductance above T_{curie} is about half the L_{eq} at room temperature. As shown in Fig. 3, in the μ_r range of the material, the changes in L_{eq} are not as significant as in the other parameters, so its variation is more gradual and even the small changes in μ_r, that occur at about 80 °C below the alloy's Curie temperature, are reflected.

However, as can be seen in Fig. 11, the R_{eq} remains constant until the prototypes heat up and approach their T_{Curie}, where the equivalent resistance drops considerably with temperature, reaching its minimum once T_{Curie} is exceeded.

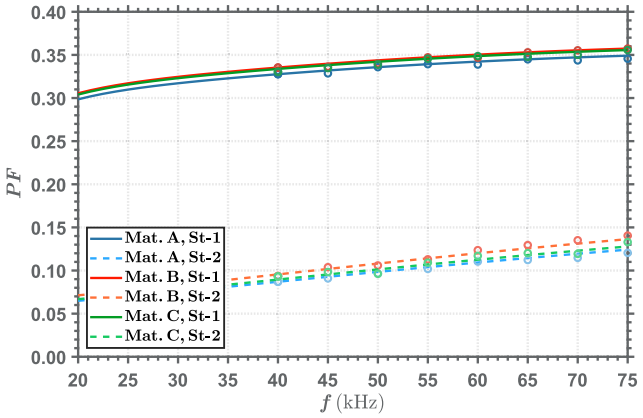

FIGURE 12. Dependence of PF with frequency at different load states. St-1 at room temperature and St-2 when T_{Curie} is exceeded.

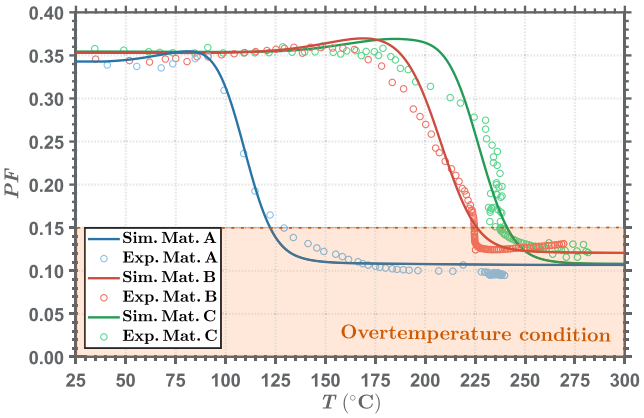

FIGURE 13. Dependence of PF on temperature at $f = 60$ kHz.

This change occurs within a small temperature range around T_{Curie}, which allows separating the operation of the load into two states. A first state, in which the high R_{eq} allows to efficiently heat up the vessel and a second state in which the R_{eq} and thus its heating capacity decrease considerably, in which the load temperature increment is limited.

The R_{eq} and L_{eq} are strongly frequency dependent, so using these parameters in the overtemperature detection implies defining a threshold for which the safety temperature is considered to be exceeded at each of the possible operating frequencies. Therefore, as in the case of vessel detection, it is also possible to use the power factor for overtemperature detection. In Fig. 12, it is shown how, within the range of use of the application (20 - 75 kHz), the PF hardly varies with frequency and, regardless of this, the two states of the load are clearly distinguishable. Based on the experimental results shown in Fig. 13 and the analysis performed on Fig. 3 (c), it is possible to define a threshold power factor of 0.15 below which it is considered that the vessel has exceeded its limit temperature and therefore is necessary to activate the protection system. This threshold can be easily included in the current cooktop digital controllers.

In induction heating the cookware does not heat up uniformly because there are areas, depending on the geometry of the inductor used by the cooktop, where more magnetic field is concentrated and therefore heat up more and faster [4]. Thus, the temperature shown in the experimental results corresponds to the maximum temperature measured in the vessel. However, the simulations performed using the analytical model shown in the previous section considers that the load is uniformly heated, which causes slight variations between the experimental and analytical models when the load approaches the Curie temperature. In any case, considering the high thermal conductivity of the involved metals, which uniformizes the temperature profile, the model accurately fits the initial and final states which are the most interesting in this study.

V. CONCLUSION

The use of multilayer loads, with a low Curie temperature materials on the bottom and an aluminum layer on top, together with the definition of a power factor threshold value, provides a reliable overtemperature detection method in DIH and self-limits the temperature rise. The Curie temperature of the material used in the first layer, which can be modified by slightly modifying the alloy composition, gives the value of the safety temperature. Once they exceed this temperature, all these alloys have been found to have similar behavior in the multilayer structure and cause similar changes in the equivalent circuit parameters. As a result, a standard power factor threshold can be set to denote the overtemperature condition and, therefore, depending on the application or cooking process for which they are intended, loads with different Curie layers and hence safety temperatures, can be manufactured.

The method for protection against high temperatures shares the same principle as automatic vessel detection, which is already integrated in current induction cooktops, adding self-protection functionality against overtemperature to the cooktop power electronics and can be integrated directly into any induction cooktop without modifying its hardware, reducing its complexity and costs.

Finally, from the experimental measurements performed with the prototypes, it has been observed that there are significant changes in the power factor of the equivalent circuit with respect to the temperature of the cookware, so the power factor can be considered a valid parameter for the detection of overtemperature. Additionally, a threshold value of power factor has been proposed, which can be straightforwardly implemented in the current induction heating technology and, below which it is considered that the system has exceeded the safety temperature.

REFERENCES

[1] Ó. Lucía, P. Maussion, E. J. Dede, and J. M. Burdío, "Induction heating technology and its applications: Past developments, current technology, and future challenges," *IEEE Trans. Ind. Electron.*, vol. 61, no. 5, pp. 2509–2520, May 2014.

[2] J. Acero, J. Burdío, L. Barragán, D. Navarro, R. Alonso, J. García, F. Monterde, P. Hernández, and S. L. I. Garde, "Domestic induction appliances," *IEEE Ind. Appl. Mag.*, vol. 16, no. 2, pp. 39–47, Mar. 2010.

[3] I. Lope, J. Acero, and C. Carretero, "Analysis and optimization of the efficiency of induction heating applications with Litz-wire planar and solenoidal coils," *IEEE Trans. Power Electron.*, vol. 31, no. 7, pp. 5089–5101, Jul. 2016.

[4] L. Meng, K. W. E. Cheng, and K. W. Chan, "Systematic approach to high-power and energy-efficient industrial induction cooker system: Circuit design, control strategy, and prototype evaluation," *IEEE Trans. Power Electron.*, vol. 26, no. 12, pp. 3754–3765, Dec. 2011.

[5] O. Lucia, J. Acero, C. Carretero, and J. M. Burdio, "Induction heating appliances: Toward more flexible cooking surfaces," *IEEE Ind. Electron. Mag.*, vol. 7, no. 3, pp. 35–47, Sep. 2013.

[6] H. Sarnago, P. Guillen, J. M. Burdio, and O. Lucia, "Multiple-output ZVS resonant inverter architecture for flexible induction heating appliances," *IEEE Access*, vol. 7, pp. 157046–157056, 2019.

[7] F. Forest, E. Laboure, F. Costa, and J. Y. Gaspard, "Principle of a multi-load/single converter system for low power induction heating," *IEEE Trans. Power Electron.*, vol. 15, no. 2, pp. 223–230, Mar. 2000.

[8] J. Acero, C. Carretero, I. Millán, Ó. Lucía, R. Alonso, and J. M. Burdío, "Analysis and modeling of planar concentric windings forming adaptable-diameter burners for induction heating appliances," *IEEE Trans. Power Electron.*, vol. 26, no. 5, pp. 1546–1558, May 2011.

[9] M. Ahrens, "Home cooking fires," Nat. Fire Protection Assoc., Quincy, MA, USA, Tech. Rep., Jul. 2020. [Online]. Available: https://www.nfpa.org/News-and-Research/Data-research-and-tools/U.S.-Fire-Problem/Home-Cooking-Fires

[10] D. Paesa, S. Llorente, C. Sagues, and O. Aldana, "Adaptive observers applied to pan temperature control of induction hobs," *IEEE Trans. Ind. Appl.*, vol. 45, no. 3, pp. 1116–1125, May 2009.

[11] U. Has and D. Wassilew, "Temperature control for food in pots on cooking hobs," *IEEE Trans. Ind. Electron.*, vol. 46, no. 5, pp. 1030–1034, Oct. 1999.

[12] K. K. Wong and N. K. Fong, "Experimental study of induction cooker fire hazard," in *Procedia Engineering*, vol. 52. Amsterdam, The Netherlands: Elsevier, 2013, pp. 13–22.

[13] E. Plumed, I. Lope, and J. Acero, "Induction heating adaptation of a different-sized load with matching secondary inductor to achieve uniform heating and enhance vertical displacement," *IEEE Trans. Power Electron.*, vol. 36, no. 6, pp. 6929–6942, Jun. 2021.

[14] C. Franco, J. Acero, R. Alonso, C. Sagues, and D. Paesa, "Inductive sensor for temperature measurement in induction heating applications," *IEEE Sensors J.*, vol. 12, no. 5, pp. 996–1003, May 2012.

[15] E. Imaz, R. Alonso, C. Heras, I. Salinas, E. Carretero, and C. Carretero, "Infrared thermometry system for temperature measurement in induction heating appliances," *IEEE Trans. Ind. Electron.*, vol. 61, no. 5, pp. 2622–2630, May 2014.

[16] A. Bono-Nuez, B. Martin-del-Brio, C. Bernal-Ruiz, F. J. Perez-Cebolla, A. Martinez-Iturbe, and I. Sanz-Gorrachategui, "The inductor as a smart sensor for material identification in domestic induction cooking," *IEEE Sensors J.*, vol. 18, no. 6, pp. 2462–2470, Mar. 2018.

[17] O. Lucia, D. Navarro, P. Guillen, H. Sarnago, and S. Lucia, "Deep learning-based magnetic coupling detection for advanced induction heating appliances," *IEEE Access*, vol. 7, pp. 181668–181677, 2019.
[18] J. Villa, D. Navarro, A. Dominguez, J. I. Artigas, and L. A. Barragan, "Vessel recognition in induction heating appliances—A deep-learning approach," *IEEE Access*, vol. 9, pp. 16053–16061, 2021.
[19] A. Pascual, J. Acero, J. M. Burdio, S. Llorente, and C. Carretero, "Self-protection systems for domestic induction heating based on ferromagnetic materials with low Curie temperature," in *Proc. IEEE 31st Int. Symp. Ind. Electron. (ISIE)*, Jun. 2022, pp. 314–319.
[20] J. Acero, R. Alonso, J. M. Burdio, L. A. Barragan, and D. Puyal, "Analytical equivalent impedance for a planar circular induction heating system," *IEEE Trans. Magn.*, vol. 42, no. 1, pp. 84–86, Oct. 2006.
[21] L. Qiu, Y. Li, Y. Yu, A. Abu-Siada, Q. Xiong, X. Li, L. Li, P. Su, and Q. Cao, "Electromagnetic force distribution and deformation homogeneity of electromagnetic tube expansion with a new concave coil structure," *IEEE Access*, vol. 7, pp. 117107–117114, 2019.
[22] L. Qiu, N. Yi, A. Abu-Siada, J. Tian, Y. Fan, K. Deng, Q. Xiong, and J. Jiang, "Electromagnetic force distribution and forming performance in electromagnetic forming with discretely driven rings," *IEEE Access*, vol. 8, pp. 16166–16173, 2020.
[23] J. Acero, I. Lope, C. Carretero, and J. M. Burdio, "Analysis and modeling of the forces exerted on the cookware in induction heating applications," *IEEE Access*, vol. 8, pp. 131178–131187, 2020.
[24] L. Qiu, W. Zhang, A. Abu-Siada, G. Liu, C. Wang, Y. Wang, B. Wang, Y. Li, and Y. Yu, "Analysis of electromagnetic force and formability of tube electromagnetic bulging based on convex coil," *IEEE Access*, vol. 8, pp. 33215–33222, 2020.
[25] J. Acero, R. Alonso, L. A. Barragan, and J. M. Burdio, "Modeling of planar spiral inductors between two multilayer media for induction heating applications," *IEEE Trans. Magn.*, vol. 42, no. 11, pp. 3719–3729, Nov. 2006.
[26] C. Carretero, R. Alonso, J. Acero, and J. M. Burdio, "Coupling impedance between planar coils inside a layered media," *Prog. Electromagn. Res.*, vol. 112, pp. 381–396, 2011.
[27] J. Acero, C. Carretero, I. Lope, R. Alonso, Ó. Lucia, and J. M. Burdio, "Analysis of the mutual inductance of planar-lumped inductive power transfer systems," *IEEE Trans. Ind. Electron.*, vol. 60, no. 1, pp. 410–420, Jan. 2013.
[28] E. Plumed, I. Lope, and J. Acero, "Modeling and design of cookware for induction heating technology with balanced electromagnetic and thermal characteristics," *IEEE Access*, vol. 10, pp. 83793–83801, 2022.
[29] A. Iorga, M. Codescu, R. Saban, and E. Patroi, "Low Curie temperature in Fe-Cr-Ni-Mn alloys," *UPB Sci. Bull., Ser. B, Chem. Mater. Sci.*, vol. 73, pp. 195–202, Jan. 2011.
[30] A. Pascual, J. Acero, C. Carretero, and S. Llorente, "Experimental characterization of materials with controlled Curie temperature for domestic induction heating applications," in *Proc. SPIEIECON Proc. Ind. Electron. Conf.*, Oct. 2021, pp. 1–6.
[31] A. Huang, H. Kim, H. Zhang, Q. He, D. Pommerenke, and J. Fan, "An impedance converter-based probe characterization method for magnetic materials' loss measurement," *IEEE J. Emerg. Sel. Topics Power Electron.*, vol. 10, no. 3, pp. 3045–3054, Jun. 2022.
[32] O. Jimenez, O. Lucia, I. Urriza, L. A. Barragan, and D. Navarro, "Power measurement for resonant power converters applied to induction heating applications," *IEEE Trans. Power Electron.*, vol. 29, no. 12, pp. 6779–6788, Dec. 2014.

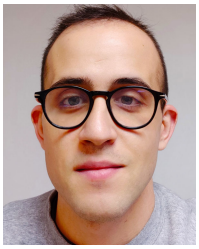

A. PASCUAL (Graduate Student Member, IEEE) received the M.Sc. degree in electronic systems engineering from the Polytechnic University of Madrid, Spain, in 2016, and the degree in industrial technologies engineering from the University of Zaragoza, where he is currently pursuing the Ph.D. degree. His main research interests include the analysis and development of advanced technologies for induction heating focused on self-protection. He is a member of the Power Electronics and Microelectronics Group (GEPM), Instituto de Investigación en Ingeniería de Aragón (I3A).

J. ACERO (Senior Member, IEEE) received the M.Sc. and Ph.D. degrees in electrical engineering from the University of Zaragoza, Zaragoza, Spain, in 1992 and 2005, respectively. From 1992 to 2000, he worked in several industry projects, especially focused on custom power supplies for research laboratories. Since 2000, he has been with the Department of Electronic Engineering and Communications, University of Zaragoza, where he is currently a Professor. His main research interests include resonant converters for induction heating applications, inductive-type load modeling, and electromagnetic modeling. He is a member of the IEEE Power Electronics Society, IEEE Industrial Electronics Society, and IEEE Magnetics Society. He is also a member of the Instituto de Investigación en Ingeniería de Aragón (I3A).

S. LLORENTE received the M.Sc. and Ph.D. degrees in electronic engineering from the University of Zaragoza, Zaragoza, Spain, in 2001 and 2016, respectively. In 2001, he joined Bosch-Siemens Home Appliances Group, Zaragoza, where he has held different positions in the Research and Development Department of Induction Cooktops. He is currently an in charge of several research lines and preprojects and also an inventor in more than 200 patents. He has also been an Assistant Professor with the University of Zaragoza, since 2004. His research interests include power electronics, simulation and control algorithms for power electronics, and temperature.

C. CARRETERO (Senior Member, IEEE) received the dual B.Sc. and M.Sc. degrees in physics and in electrical engineering and the Ph.D. degree in electrical engineering from the University of Zaragoza, Zaragoza, Spain, in 1998, 2002, and 2010, respectively. He is currently an Assistant Professor with the Department of Applied Physics, University of Zaragoza. His research interests include induction heating applications and electromagnetic modeling of inductive systems. He is a member of the Instituto de Investigación en Ingeniería de Aragón (I3A).

J. M. BURDIO (Senior Member, IEEE) received the M.Sc. and Ph.D. degrees in electrical engineering from the University of Zaragoza, Zaragoza, Spain, in 1991 and 1995, respectively. In 2000, he was a Visiting Professor at the Center for Power Electronics Systems, Virginia Tech. He has been with the Department of Electronic Engineering and Communications, University of Zaragoza, where he is currently a Professor, the Head of the Group of Power Electronics and Microelectronics, and the Director of the BSH Power Electronics Laboratory with the University of Zaragoza. He is the author of more than 80 international journal articles and over 200 papers in conference proceedings and the holder of more than 60 international patents. His main research interests include modeling of switching converters and resonant power conversion for induction heating and biomedical applications. He is a Senior member of the Power Electronics and Industrial Electronics Societies. He is also a member of the Instituto de Investigación en Ingeniería de Aragón (I3A).